Nature of magnetic domains in an exchange coupled $BiFeO_3$/CoFe heterostructure

Cite as: Appl. Phys. Lett. **102**, 112902 (2013); https://doi.org/10.1063/1.4795794
Submitted: 21 January 2013 . Accepted: 06 March 2013 . Published Online: 19 March 2013

D. Y. Qiu, K. Ashraf, and S. Salahuddin

Nature of magnetic domains in an exchange coupled $BiFeO_3$/CoFe heterostructure

D. Y. Qiu,[1] K. Ashraf,[2] and S. Salahuddin[2,a)]
[1]*Department of Physics, University of California, Berkeley, California 94720, USA*
[2]*Department of Electrical Engineering and Computer Sciences, University of California, Berkeley, California 94720, USA*

(Received 21 January 2013; accepted 6 March 2013; published online 19 March 2013)

We use the micromagnetic model to simulate magnetization in a multidomain $BiFeO_3$(BFO)/CoFe bilayer. We show that CoFe couples to weak ferromagnetism on the BFO surface and breaks into domains that correspond exactly with BFO domains. Switching the direction of the BFO spins switches the corresponding CoFe domains and reverses the net magnetization. Since magnetization is coupled to polarization in BFO, this demonstrates a mechanism for controlling magnetization reversal with an electric field. Comparison with experimental values of BFO surface moment and hysteresis allows us to extract BFO/CoFe exchange and spin canting energies and predict behavior for domains of varying sizes. © *2013 American Institute of Physics*. [http://dx.doi.org/10.1063/1.4795794]

$BiFeO_3$ (BFO) is a magnetoelectric multiferroic that exhibits both ferroelectric (FE) and antiferromagnetic (AFM) ordering at room temperature. As such, it has generated considerable interest because of potential applications in low-power devices where the magnetization state can be switched by an electric field. Density Functional Theory (DFT) studies of BFO indicate that the magnetization lies in a plane perpendicular to the polarization, **P** (Figure 1(a)).[1] Canting of the antiferromagnetic moments, due to the Dzyaloshinskii-Moriya (DM) effect, gives rise to weak ferromagnetism in the magnetization plane.[1–3] This perpendicular relationship between **P** and the magnetization plane suggests that in a monodomain, the maximum magnetic switching is 90°, corresponding to maximum rotation of the magnetization plane (Figure 1(b)). However, Heron *et al*. have demonstrated that electric-field induced 180° net magnetization reversal may be possible in a multi-domain material, with a stripe-like domain pattern, where each domain switches by 90°.[4] They grew a Pt(2.5 nm)/$Co_{0.9}Fe_{0.1}$(2.5–3 nm)/BFO(70–100 nm) heterostructure. The BFO had 200 nm-wide stripe-like domains, where the in-plane polarization in each domain alternated between 45° and −45° to the net in-plane polarization, $\mathbf{P}_{net-IP}$ (Figure 1(c)). Photo Emission Electron Microscopy (PEEM) images showed that CoFe grown on the (001)-surface of BFO broke into magnetic domains with a roughly one-to-one correspondence to the FE domains in BFO (Figure 1(d)). An electric field reversed $\mathbf{P}_{net-IP}$ by switching polarization in each domain by 90° (Figure 1(e)). AMR measurements indicate that the net magnetization also switched reversibly by 180°, when the electric field was applied. This suggests that the magnetic domains in BFO follow the FE domains as they switch, but the switching behavior of the individual magnetic domains was not directly observed. We use micromagnetic simulations to show that a one-to-one correspondence between magnetization and polarization switching in BFO is indeed possible depending on the degree of spin canting, the switching speed, the domain size, and the strength of the exchange interaction between the FM and the AFM.

While DFT simulations indicate that bulk BFO has three degenerate easy magnetization axes in the (111) plane, epitaxially straining BFO lifts the degeneracy of the magnetization axis.[5] However, the direction of the resulting magnetization axis is not conclusively known and could be along either $[1\bar{1}0]$ or $[11\bar{2}]$. For our simulations, the one-to-one correspondence between FE and FM domains seen in Ref. 4 allows us to make a reasonable guess for the magnetization axis. The one-to-one correspondence is surprising since the 200 nm FE domains are considerably smaller than typical domain sizes of 1–10 μm in antiferromagnetically coupled multilayers.[6] We would expect one-to-one behavior if the polarization couples strongly with the anisotropy easy-axis of the AFM spins in BFO, thus fixing the AFM domains in the same area as the FE domains. Then, canting of the AFM spins would create a net magnetic moment that can couple with the FM, creating ferromagnetic domains in the same area as the ferroelectric domains. Figure 1(f) describes the directions of the polarization and magnetic moments on the (001)-surface of BFO in such a scheme. Within the assumption of exchange interaction, BFO couples antiferromagnetically to the ferromagnet. Then the in-plane projection of the canted moment, $\mathbf{M_{IP}}$, should be anti-parallel to the in-plane projection of the polarization, $\mathbf{P_{IP}}$. Thus, if the polarization, **P**, is along [111], the in-plane projection of the canted moment should be along $[1\bar{1}0]$. The actual spin canting direction is perpendicular to both **P** and the AFM easy axis, **L** (which lies in the (111) plane).[1] This means that the canted moment, **M**, must lie in the (111) plane, so in order to have the desired in-plane projection, **M** should lie along $[11\bar{2}]$. If **M** is along $[11\bar{2}]$, then the AFM easy axis, **L**, which is perpendicular to **M**, must lie along $[1\bar{1}0]$. This reasoning is consistent with experiments which suggest that epitaxially strained BFO has magnetic moments along $[11\bar{2}]$.[5]

We use the Object Oriented Micromagnetic Framework (OOMMF)[7] to reproduce experimental results from Ref. 4, based on the assumptions that the polarization fixes the direction of the AFM easy-axis in BFO and that spin canting

a)Author to whom correspondence should be addressed. Electronic mail: sayeef@eecs.berkeley.edu

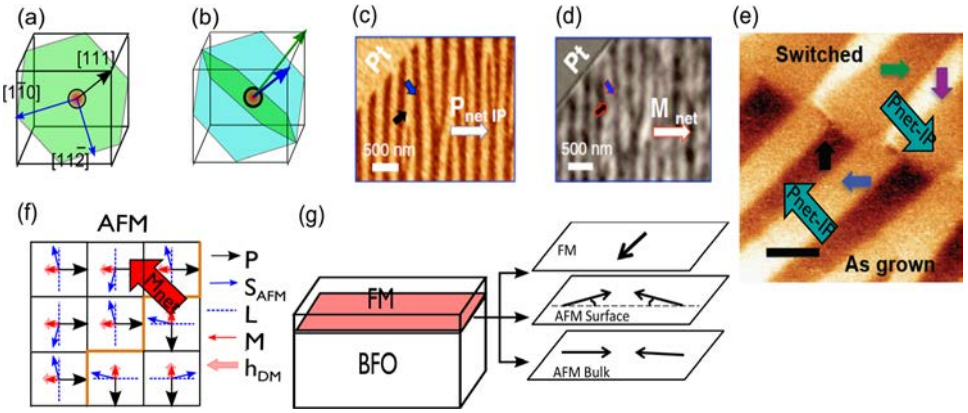

FIG. 1. Model for magnetization switching in BFO. (a) Schematic of oxygen-centered BFO unit cell with polarization (black arrow) along [111] and easy magnetization plane. Blue arrows indicate possible magnetization directions in the plane. (b) Switching of the magnetization plane induced by 71° polarization switching. (c) In-plane PFM images of BFO ferroelectric domains. (d) XMCD-PEEM images of magnetic moments in CoFe. (c), (d) The blue (gray) and black arrows correspond to in-plane projections of BFO polarization and CoFe magnetic moment in each domain. (e) In-plane PFM image of BFO with regions of as-grown and reversed polarization domains. Observe that 90° polarization switching of each domain results in 180° net polarization switching. (f) Schematic of polarization and magnetization on the (001) surface of BFO. The orange line highlights a 90° domain wall. The direction of the spin, $\mathbf{S}_{AFM}$, in each unit cell is represented by the solid blue arrow. Each spin is canted away from the AFM easy axis, **L**, by the field $\mathbf{h}_{DM}$ resulting in a weak ferromagnetic moment along the small red arrow, **M**. This creates net magnetization, $\mathbf{M}_{net}$, along the diagonal. (g) Schematic of simulated BFO/FM bilayer with close-up of interface region. At the interface, the FM spins couple antiferromagnetically with canted spins on the BFO surface. (c), (d), (e) are reprinted with permission from J. T. Heron, M. Trassin, K. Ashraf, M. Gajek, Q. He, S. Y. Yang, D. E. Nikonov, Y.-H. Chu, S. Salhuddin, and R. Ramesh, Phys. Rev. Lett. **107**, 217202 (2011). Copyright 2011 American Physical Society.

in BFO creates net magnetic moment that couples to CoFe. OOMMF uses the Euler method to solve the Landau-Lifshitz-Gilbert (LLG) equation

$$\frac{d\mathbf{M}}{dt} = -|\gamma|\mathbf{M} \times \mathbf{H}_{eff} + \frac{\alpha}{M_S}\left(\mathbf{M} \times \frac{d\mathbf{M}}{dt}\right), \qquad (1)$$

where **M** is the magnetization, α is the damping, γ is the gyromagnetic ratio, M_S is the saturation magnetization, and $\mathbf{H}_{eff}$ is the effective magnetic field. We setup a simulation with a 10 nm thick ferromagnet (FM) on the (001)-surface of a 100 nm thick AFM (Figure 1(g)). Contributions to $\mathbf{H}_{eff}$ are (1) demagnetization energy, (2) K_{AFM}, the AFM uniaxial anisotropy energy, (3) J_{AFM}, J_{FM}, and J_{int}, the nearest-neighbor exchange stiffness between spins in the AFM, in the FM, and at the AFM/FM interface, and (4) $\mathbf{h_{DM}}$ is a magnetic field applied to the AFM at the AFM/FM interface to simulate spin-canting due to the DM effect. This follows from Ref. 8, which indicates that the DM effect can be modeled by a uniform field along the direction of $\mathbf{P} \times \mathbf{L}$, at the interface between a FM and a G-type AFM. The parameters for the FM(CoFe) are $M_S = 1.592 \times 10^6$ A/m and $J_{FM} = 3 \times 10^{-11}$ J/m.[4,9] The parameters for the AFM(BFO) are $M_S = 4.26 \times 10^5$ A/m, $K_{AFM} = 1.75 \times 10^4$ J/m^3, and $J_{AFM} = -2.6 \times 10^{-12}$ J/m.[1,10,11] Values for J_{int} and $\mathbf{h}_{DM}$ are unknown; we vary J_{int} and $\mathbf{h}_{DM}$ and compare our simulation results with experimental results to obtain physical values for J_{int} and $\mathbf{h}_{DM}$ in BFO.

To create the domain pattern from Ref. 4, AFM domains with 71° domain walls were imposed by fixing K_{AFM} along different directions in neighboring domains, as in Figure 1(f). **L**, the direction of K_{AFM}, is along [110] in one domain and [1$\bar{1}$0] in the neighboring domain. Similarly, $\mathbf{h}_{DM}$, which sets the direction of the canted moment **M**, is along [$\bar{1}$1$\bar{2}$] in one domain and [11$\bar{2}$] in the neighboring domain. These directions were chosen to give magnetization parallel to polarization, as seen in Ref. 4, but the results of the simulation depend only on the relative angles between $\mathbf{h}_{DM}$ and **L**. The mesh size used in the simulation is 10 nm by 10 nm by 10 nm. We ran simulations with AFM domain widths of 50 nm, 100 nm, and 200 nm.

We assume that both $\mathbf{h}_{DM}$ and **L** rotate by 90° in-plane when the polarization rotates by 90°. We want to model how the FM responds to FE switching for different values of J_{int} and $\mathbf{h}_{DM}$. To simulate this process, we relax the AFM/FM bilayer, starting from the assumption that $\mathbf{h}_{DM}$ and **L**, in the AFM, have already switched while the FM has not. The bilayer relaxes from an initial configuration where each FM domain is aligned along the direction of **L** in the AFM domain directly beneath it, and the net magnetization of the FM is parallel to the net magnetization of the AFM (Figure 2(a)). To reproduce experimental behavior the net FM magnetization must switch by 180°.

Depending on the J_{int} and $\mathbf{h}_{DM}$ parameters, the AFM/FM bilayer relaxation displays one of three types of behavior (Figures 2(c)–2(e)). Figure 2(b) is a phase diagram of the angle between the final and initial net FM magnetization, when the AFM domains are 200 nm wide. The red region indicates the parameters that result in 180° switching, thus reproducing experimental behavior. In this region, each FM domain switches by 90°, and $\mathbf{M}_{net-IP}$ switches by 180° (Figure 2(c)). The AFM remains in the initial configuration so the FM domains have switched to be anti-parallel to the AFM canted moment. The blue region in the phase diagram corresponds to no switching of the net FM magnetization. For these parameters, each FM domain still switches by 90°, but the direction of the net magnetization does not change (Figure 2(e)). The direction of spin canting in each AFM domain reverses by 180°, so coupling with the FM has destroyed the preferential canting direction imposed by $\mathbf{h}_{DM}$. In the remaining parts of the phase diagram, the net FM magnetization rotates by less than 180°. In these regions, the FM and AFM break into smaller domains, and the original stripe-

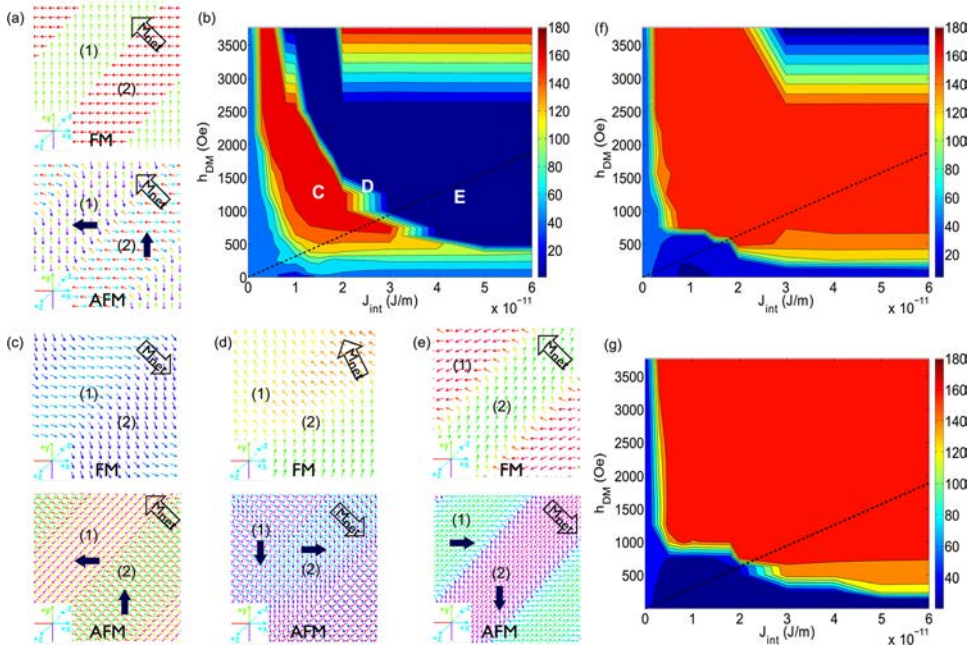

FIG. 2. (a) Initial state of the FM and AFM spins in the simulations. The solid blue arrows indicate the directions of net magnetization in each AFM domain. Corresponding domains in the FM and AFM are labeled 1 and 2. The same labeling scheme is used in (c)-(e). (b) Phase diagram of the angle (in degrees) between the final and initial net FM magnetization for different J_{int} and $\mathbf{h}_{DM}$ parameters when the AFM domain size is 200 nm. An angle of 180° (the red region) indicates magnetization reversal. The regions labeled C, D, and E have final spin configurations that correspond with (c), (d), and (e). The dashed line represents a limit on J_{int} with respect to $\mathbf{h}_{DM}$ above which exchange bias is expected. (c) Final state of FM and AFM spins with parameters corresponding to region C in the phase diagram. The net FM magnetization has switched by 180°. The net AFM magnetization remains unchanged. (d) Final state of FM and AFM spins with parameters corresponding to region D in the phase diagram. The stripe-like domain structure is destroyed. (e) Final state of FM and AFM spins with parameters corresponding to region E in the phase diagram. The net AFM magnetization has switched by 180°. The net FM magnetization remains unchanged. (f) Phase diagram of the angle between the final and initial net FM magnetization when the AFM domain size is 100 nm. (g) Phase diagram of the angle between the final and initial net FM magnetization when the AFM domain size is 50 nm.

like domain pattern is lost (Figure 2(d)). The direction of the net FM magnetization tends to point along the direction of the easy-axis determined by the FM's shape anisotropy. The AFM spins are canted in a direction anti-parallel to the FM spins. As J_{int} approaches zero, the stripe-like FM domain pattern disappears, and the net FM magnetization points along the direction determined by the FM's shape anisotropy.

As the AFM domains become narrower, the region of the phase diagram that corresponds to 180° magnetization switching becomes larger. Figures 2(f) and 2(g) are a phase diagrams of the angle between the final and initial net FM magnetization for 100 nm and 50 nm domains. As the domain size decreases, the angle between magnetization in neighboring domains decreases from 90° in bilayers with 200 nm domains to less than 30° in bilayers with 50 nm domains.

The surface magnetic moment of (001)-BFO has been measured between 0.06 and 1 μ_B per unit cell,[12–14] and experimental measurements place the magnetic moment of BFO at the BFO/LSMO interface at ~0.6 μ_B per unit cell.[15] This is a critical metric that could potentially provide important insights into J_{int} and $\mathbf{h}_{DM}$. However, it is difficult to directly compare with experimental values of surface moment because of the uncertainty of how many layers inside the AFM are actually probed while doing the surface measurement. To illustrate this problem, we show the behavior of magnetic moment in the AFM as a function of distance from the surface (see Figure 3). Note that the moment shows a decaying sinusoidal variation with a rapid decline in the first 20 nanometers. The average magnetization inside the first 20 nm is much smaller (almost a factor of 2) than the peak value of the magnetization. Due to this reason, in our discussion hereafter, we shall only mention the peak value of the AFM magnetization μ_s^{peak}, considering that the actual average magnetization (and therefore the values probed by the experiment) could be lower.

Figure 4(a) indicates the μ_s^{peak} of the interface layer of an AFM with 200 nm domains, for different values of J_{int} and $\mathbf{h}_{DM}$. In the absence of a FM, the surface moment is on the order of 0.01 μ_B per unit cell. The net magnetization is between 0.5 and 3.0 μ_B per unit cell for the range of parameters that reproduce the experimental domain pattern, so the exchange interaction between the AFM and the FM significantly enhances the AFM surface moment in keeping with what has been observed experimentally. Smaller domain sizes also tend to increase the net interface magnetization (Figure 4(b)). For $\mathbf{h}_{DM}$ and J_{int} parameters that result in 180° magnetization switching, there is approximately a linear relationship between the AFM interface magnetization and the energy density (Figure 4(d)). The energy density of a single AFM spin, $\vec{S}_i^{AFM}$, at the interface can be roughly described by

$$E_i = -\frac{J_{int}}{A}\vec{S}_i^{AFM}\cdot\vec{S}_j^{FM} - \mu_0 M_S^{BFO}\vec{S}_i^{AFM}\cdot\vec{h}_{DM} - K_{AFM}\sin^2\theta - \frac{J_{AFM}}{A}\sum_j \vec{S}_i^{AFM}\cdot\vec{S}_j^{AFM}, \quad (2)$$

where $\vec{S}_i$ is a normalized vector along the direction of the spin, M_S^{BFO} is the saturation magnetization of BFO, K_{AFM} is

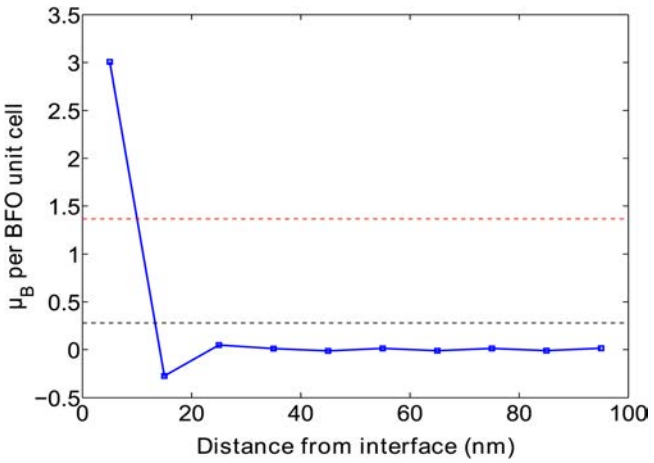

FIG. 3. Plot of AFM magnetization vs. the distance from the AFM/FM interface. The red (upper) dashed line is the average magnetization within 20 nm of the interface. The black (lower) dashed line is the average magnetization of the entire AFM.

the anisotropy energy, θ is the angle from the anisotropy axis, A is the area of each spin, J_{AFM} is the AFM exchange stiffness, and the index j refers to the nearest neighbors of i. Assuming that $\vec{S}_i^{FM}$ is approximately antiparallel to $\vec{h}_{DM}$ and neglecting exchange with the bulk, Eq. (2) becomes

$$E_i = -\frac{J_{\text{int}}}{A}\frac{M_{AFM}}{M_S^{BFO}} + \mu_0|\vec{h}_{DM}|M_{AFM} - K_{AFM}\left(\frac{M_{AFM}}{M_S^{BFO}}\right)^2 - 4\frac{J_{AFM}}{A}\left[1-\left(\frac{M_{AFM}}{M_S^{BFO}}\right)^2\right], \quad (3)$$

where M_{AFM} is the canted moment. Minimizing and solving for M_{AFM} gives

$$M_{AFM} = 2(M_S^{BFO})^2\left(K_{AFM} - 4\frac{J_{AFM}}{A}\right) \times \left(-\frac{J_{\text{int}}}{A}\frac{1}{M_S^{BFO}} + \mu_0|\vec{h}_{DM}|\right). \quad (4)$$

M_{AFM} versus $(-\frac{J_{\text{int}}}{A} + M_S^{BFO}\mu_0|\vec{h}_{DM}|)$ is plotted in Figure 4(d), the best linear fit has a slope of 1.26×10^{-5} $\mu_B/(J/m^3)$, which is well-estimated by 0.91×10^{-5} $\mu_B/(J/m^3)$, the slope in Eq. (4). This model also explains why the magnetic moment is higher in materials with smaller domains. When the domains are smaller, the FM spins deviate more from the direction of $\vec{h}_{DM}$, thus increasing the energy due to the $\frac{J_{\text{int}}}{A}\vec{S}_i^{AFM}\cdot\vec{S}_j^{FM}$ term. Since surface moment goes linearly with energy, this increases the surface moment.

We can further limit the allowed phase space for values of J_{int} and $\mathbf{h}_{DM}$ by fitting the behavior of the coercive field to experimental results. No exchange bias is observed in the BFO/CoFe heterostructure.[4] Hence, we can limit the allowed phase space of J_{int} and $\mathbf{h}_{DM}$ by noting that we expect exchange bias in systems where[16]

$$J_{ex} > 1/2 H_{K,AFM} M_{FM} t_{FM}. \quad (5)$$

$H_{K,AFM}$ is the anisotropy field of AFM magnetic moment, which we take to be $\mathbf{h}_{DM}$, and J_{ex} is the interface exchange energy per unit area. Applying this relation, the allowed values of J_{int} and $\mathbf{h}_{DM}$ fall below the dashed line in the phase diagrams. We use OOMMF to calculate the coercive field using 200 nm domains and the same parameters as the previous simulations but with the uniform $\mathbf{h}_{DM}$ replaced by a uniaxial field. The experimentally measured coercive field is 50 Oe.[4] The calculated coercive field starts at 0 and increases with J_{int} until it peaks near $J_{\text{int}} = 1\times10^{-11}$ J/m

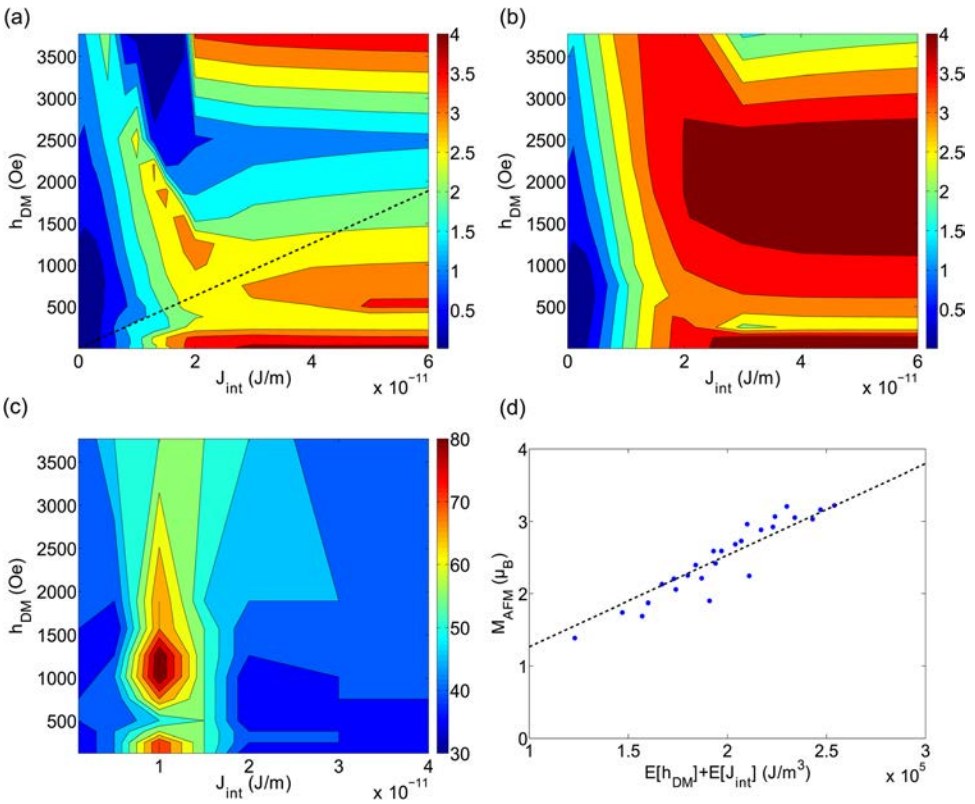

FIG. 4. (a) Phase diagram of μ_s^{peak} for different J_{int} and h_{DM} parameters when the domain size is 200 nm. The dashed line represents a limit on J_{int} with respect to h_{DM} above which exchange bias is expected. The scale is in μ_B per unit cell. (b) Phase μ_s^{peak} when the domain size is 100 nm. (c) Phase diagram of the coercive field for different J_{int} and h_{DM}. The color scale is in Oe. The domain size is 200 nm. (d) AFM surface moment in μ_B per unit cell versus energy density due to the interfacial exchange stiffness and canting field, for parameters that result in 180° magnetization reversal.

(Figure 4(c)). Reproducing both the experimental coercive field and switching behavior requires $\mathbf{h}_{DM}$ around 500 Oe and J_{int} between 1.5×10^{-11} J/m and 2.0×10^{-11} J/m. These parameters result in μ_s^{peak} of 2–3 μ_B per unit cell magnetic moment. The value for J_{int} is comparable to values for other antiferromagnetically coupled interfaces, such as Co/Ru/Co and Co/NiO, which have exchange stiffness parameters of around 2×10^{-11} J/m.[17,18]

In the previous simulations, we relaxed the AFM/FM system, starting from initial conditions where both **L** and $\mathbf{h}_{DM}$ have already switched. This neglects the fact that $\mathbf{h}_{DM}$ should be uniaxial rather than unidirectional. Next, we allow $\mathbf{h}_{DM}$ to be uniaxial and look at how switching dynamics affect the final domain pattern. In the simulations, **L** starts along $[1\bar{1}0]$ and $[\bar{1}\bar{1}0]$ in neighboring domains and moves in 10 equally spaced time steps to the final directions [110] and $[1\bar{1}0]$. $\mathbf{h}_{DM}$ is a uniaxial field perpendicular to **L**. The AFM spins start from a configuration where they have uniform spin canting in each domain. The damping parameter α is taken to be 0.01. Simulations were run for switching over 0.1 and 1.0 ns.

We find that for switching over 0.1 ns, the AFM spins lag behind the rotation of the AFM anisotropy axis, **L**. By the time **L** is done switching, both the FM and the AFM spins have not moved significantly from their initial configuration (Figures 5(a) and 5(b)). The AFM spins eventually relax to align along **L**, and the relaxed spins are canted along different directions of the uniaxial $\mathbf{h}_{DM}$ axis in different regions of the magnet. The FM breaks into domains aligned with the direction of AFM spin canting and 180° rotation is not guaranteed (Figure 5(c)).

For slower switching speeds of 1 ns, the AFM spins follow the AFM anisotropy axis during the switching process. Since the AFM spins initially have uniform canting in each domain, they remain uniformly canted as the AFM spins rotate, and the canted moment maintains a stripe-like domain pattern. The FM lags behind the AFM, but it eventually relaxes to align with the AFM canted moment (Figures 5(d)–5(f)). Thus, when the switching speed of the AFM easy axis is slow enough for the AFM spins to rotate at the same speed as the AFM easy axis, switching each domain in the AFM by 90° switches the net FM magnetization by 180°.

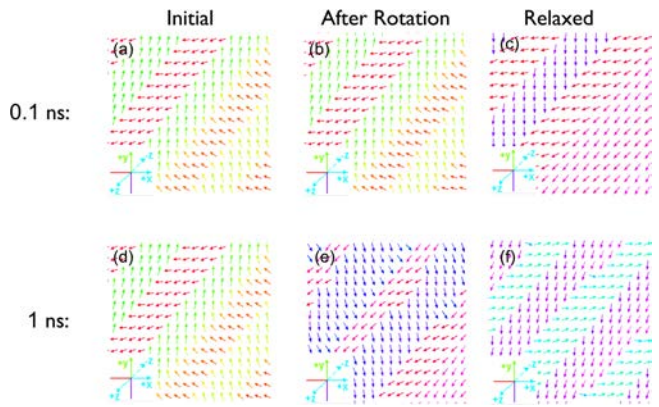

FIG. 5. (a)-(c) Magnetization of the FM during switching over 0.1 ns. (d)-(f) Magnetization of the FM during switching over 1.0 ns. The left-most figure shows the initial magnetization. The central figure shows the FM magnetization after the AFM easy axis has finished rotating. The right-most figure shows the FM magnetization after it has relaxed from the central configuration.

In summary, we used micromagnetic simulations to reproduce experimental observations of one-to-one mapping between domains in BFO and CoFe and subsequent 180° magnetization switching in a BFO/CoFe heterostructure. Our simulations are based on the assumption that coupling with the polarization fixes the easy axis of the AFM spins in each BFO domain and that spin canting in BFO creates weak ferromagnetism that couples to CoFe. This creates CoFe domains that correspond exactly with the FE domain in BFO. For sufficiently slow switching dynamics, in materials with 200 nm domains, interfacial exchange stiffness between 1.5×10^{-11} and 2×10^{-11} J/m and spin canting field around 500 Oe result in magnetization reversal and reproduce the experimental coercive field. The stripe-like magnetic domain pattern is preserved in the switched magnet and during the switching process. We observe that as the AFM domain size decreases, the angle between neighboring domains in the FM decreases, the interfacial AFM moment increases, and 180° magnetization reversal occurs for a larger range of parameters. Thus, we predict that decreasing the BFO domain size, which can be achieved by substrate strain, and changing the thickness of BFO thin film will make it easier to use polarization switching in BFO to switch the magnetization of a larger range of FM materials.

The authors would like to acknowledge many fruitful discussions with R. Ramesh, M. Trassin, and J. T. Heron. This work was supported in part by National Science Foundation under Grant No. 0939514 and Grant No. 1017575.

[1]C. Ederer and N. Spaldin, Phys. Rev. B **71**, 060401(R) (2005).
[2]I. E. Dzyaloshinskii, Sov. Phys. JETP. **5**, 1259–1272 (1957).
[3]T. Moriya, Phys. Rev. **120**, 91–98 (1960).
[4]J. T. Heron, M. Trassin, K. Ashraf, M. Gajek, Q. He, S. Y. Yang, D. E. Nikonov, Y.-H. Chu, S. Salahuddin, and R. Ramesh, Phys. Rev. Lett. **107**, 217202 (2011).
[5]M. B. Holcomb, L. W. Martin, A. Scholl, Q. He, P. Yu, C.-H. Yang, S. Y. Yang, P.-A. Glans, M. Valvidares, M. Huijben, J. B. Kortright, J. Guo, Y.-H. Chu, and R. Ramesh, Phys. Rev. B **81**, 134406 (2010).
[6]S. Langridge, J. Schmalian, C. H. Marrows, D. T. Dekadjevi, and B. J. Hickey, Phys. Rev. Lett. **85**, 4964–4967 (2000).
[7]M. J. Donahue and D. G. Porter, *OOMMF User's Guide Version 1.0* (National Institute of Standards and Technology, Gainsburg, MD, 1999).
[8]S. Dong, K. Yamauchi, S. Yunoki, R. Yu, S. Liang, A. Moreo, J.-M. Liu, S. Picozzi, and E. Dagotto, Phys. Rev. Lett. **103**, 127201 (2009).
[9]C. Bilzer, T. Devolder, J.-V. Kim, G. Counil, C. Chappert, C. Cardoso, and P. P. Freitas, J. Appl. Phys. **100**, 053903 (2006).
[10]M. Matsuda, R. S. Fishman, T. Hong, C. H. Lee, T. Ushiyama, Y. Yanagisawa, Y. Tomioka, and T. Ito, Phys. Rev. Lett. **109**, 067205 (2012).
[11]K. Ashraf and S. Salahuddin, J. Appl. Phys. **111**, 103904 (2012).
[12]H. Béa, M. Bines, S. Fusil, K. Bouzehouane, E. Jacquet, K. Rode, P. Bencok, and A. Barthélémy, Phys. Rev. B **74**, 020101(R) (2006).
[13]W. Eerenstein, F. D. Morrison, J. Dho, M. G. Blamire, J. F. Scott, and N. D. Mathur, Science **307**, 1203 (2005).
[14]J. Wang, J. B. Neaton, H. Zheng, V. Nagarajan, S. B. Ogale, B. Liu, D. Viehland, V. Vaithyanathan, D. G. Schlom, U. V. Waghmare, N. A. Spaldin, K. M. Rabe, M. Wuttig, and R. Ramesh, Science **299**, 1719–1722 (2003).
[15]P. Yu, J.-S. Lee, S. Okamoto, M. D. Rossell, M. Huijben, C.-H. Yang, Q. He, J. X. Zhang, S. Y. Yang, M. J. Lee, Q. M. Ramasse, R. Erni, Y.-H. Chu, D. A. Arena, C. C. Kao, L. W. Martin, and R. Ramesh, Phys. Rev. Lett. **105**, 027201 (2010).
[16]W. H. Meiklejohn, J. Appl. Phys. **33**, 1328–1335 (1962).
[17]E. Girt, W. Huttema, O. N. Mryasov, E. Montoya, B. Kardasz, C. Eyrich, B. Heinrich, A. Y. Dobin, and O. Karis, J. Appl. Phys. **109**, 07B765 (2011).
[18]H. Ohldag, A. Scholl, F. Nolting, E. Arenholz, S. Maat, A. T. Young, M. Carey, and J. Stöhr, Phys. Rev. Lett. **91**, 017203 (2003).